A Multi-metric Modular Framework for Human-like Gait Analysis Based on a Recorded Set of Variable Gait Patterns

Kapteijn, S.; Kim, Wansoo ; Marchal Crespo, L.; Peternel, L.

DOI
10.1109/Humanoids53995.2022.10000194

Publication date
2022

Document Version
Final published version

Published in
Proceedings of the 2022 IEEE-RAS 21st International Conference on Humanoid Robots (Humanoids)

2022 IEEE-RAS 21st International Conference on Humanoid Robots (Humanoids)
November 28-30, 2022. Ginowan, Japan.

A Multi-metric Modular Framework for Human-like Gait Analysis Based on a Recorded Set of Variable Gait Patterns

Stephan Kapteijn[1], Wansoo Kim[2], Laura Marchal-Crespo[1,3], and Luka Peternel[1*]

2022 IEEE-RAS 21st International Conference on Humanoid Robots (Humanoids) | 979-8-3503-0979-9/22/$31.00 ©2022 IEEE | DOI: 10.1109/HUMANOIDS53995.2022.10000194

***Abstract*— Walking is an essential part of almost all activities of daily living. We use different gait patterns in different situations, e.g., moving around the house, performing various sports, or when compensating for an injury. However, how humans perform this gait tailoring remains a partially unknown process. To this end, the influence of various performance metrics on the optimality and diversity of gait patterns can provide us with more insight. To analyse gait in terms of pattern diversity and performance metrics related to physical aspects, such as joint torque, fatigue, and manipulability, we propose a multi-metric gait analysis framework that simultaneously accounts for these parameters. We used a recorded set of versatile gait patterns that are already dynamically stable and physiologically feasible. To that end, 45 gait variations–varying in stride length, step height, and walking speed–were recorded in a motion capture experiment. Results of analysis using the recorded dataset are presented for a baseline case (with all optimisation weights set to one), which serves as the first step for future research, in particular giving insights into specific aspects of the gait, e.g., joint loading, long-term performance, and capacity to sustain ground reaction forces.**

I. Introduction

Bipedal walking is one of the primary forms of human transportation and is an essential part of many activities of daily living. Due to our exceptional motor learning capabilities, humans can customise their gait to achieve different goals, i.e., walk silently, avoid slipping on a wet floor, perform different sports, or compensate for an injury. However, how humans perform this gait tailoring remains a partially unknown process. This is of special interest in humanoid robotics and rehabilitation robotics, since humanoid robots [1]–[3] and assistive exoskeletons [4]–[6] try to emulate the human body structure and bipedal gait patterns.

To ensure that a certain gait pattern is optimal for the activity that we plan to perform, some kind of gait optimisation technique is required. For example, if a human or a humanoid robot needs to walk a large distance, we might want to minimise energy consumption. Alternatively, if a human or a robot suffers a joint injury/damage, we might want to minimise the loads on the injured/damaged joint during walking. Therefore, we need to carefully select several metrics to perform a specific optimisation process to achieve a set goal.

[1]Department of Cognitive Robotics, Delft University of Technology, Delft, The Netherlands.
[2]Department of Robotics, Hanyang University, Seoul, Korea.
[3]ARTORG Center for Biomedical Engineering Research, University of Bern, Switzerland.
*Corresponding author (l.peternel@tudelft.nl).

Some human-specific metrics for optimisation are of qualitative nature. For example, the method in [7] proposed a personalised gait optimisation framework based on the user's preference (in terms of comfort) to determine the optimal gait pattern. The study in [8] investigated the users' repeatability in identifying their preferred robotic assistance from a bilateral ankle exoskeleton and concluded that individuals are able to reliably identify their preferences. While qualitative metrics are important for gait customisation, they do not directly and quantitatively account for physical aspects such as joint torques, manipulability, and fatigue. Furthermore, they are obviously not applicable to humanoid robots.

Monitoring the temporal joint loads during walking is crucial to prevent musculoskeletal injuries in humans and/or prevent exceeding the maximum power capacity of robot actuators. For example, joint torques can be minimised during the gait to this effect [9], [10]. Yet, joint torques and velocities can also be optimised indirectly by analysing leg manipulability. The manipulability of an articulated mechanical system (i.e., human or robot) measures its ability to transfer joint movements/torques into endpoint movements/forces as a function of the joint configuration [11]. Thus, it gives an indication of how well an endpoint (e.g., foot) of the mechanical system can produce force or velocity in certain directions in the Cartesian space. Therefore, this metric helps determine the optimal leg configuration to support external forces, e.g., ground reaction forces (GRFs), during walking. The method in [12] used manipulability to improve the energy efficiency of human walking with an exoskeleton. The study in [13] exploited manipulability for the selection of an appropriate postural strategy to restore stability when human walking is perturbed.

While joint torque and manipulability examine instantaneous physical properties, they do not directly account for the long-term endurance of the gait. Therefore, fatigue should also be monitored to ensure that we can maintain a certain gait for long periods of time. In humans, fatigue can be indirectly accounted for by optimising energy efficiency [3], [14] or metabolic cost [10], [15], [16]. A more direct way to minimise fatigue is to use fatigue models that operate based on integrated effort over time. These models can be distinguished by how they estimate the effort, e.g., using muscle activity [17], limb endpoint force [18], or joint torque [19]–[21] in humans, and motor temperature [22] in robots. Nevertheless, fatigue models have been more commonly employed in upper limbs or whole-body analysis and control of ergonomics in manufacturing processes.

Gait analysis and optimisation have been performed using

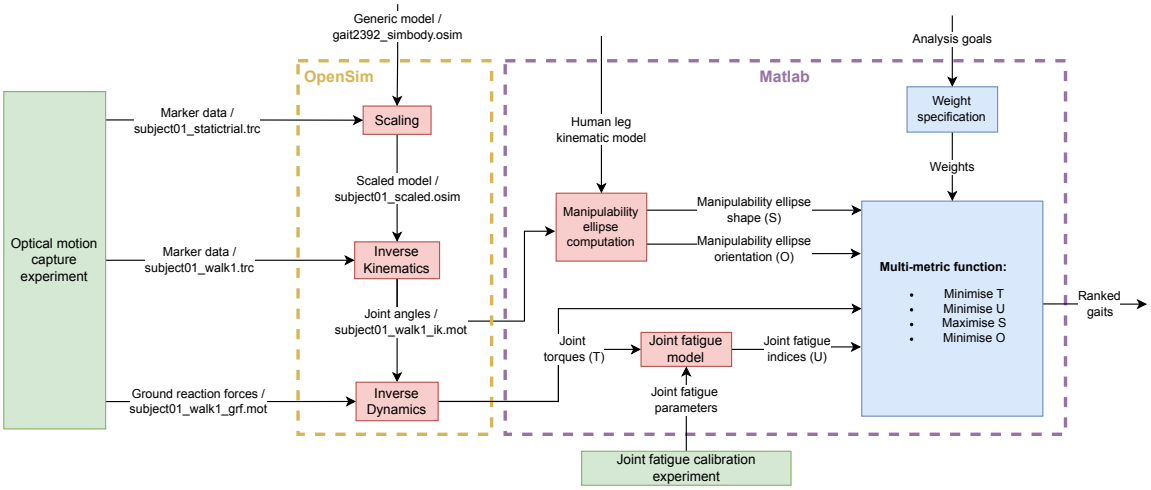

Fig. 1: Overview of the established framework, containing experiments (green), modelling/computational methods (red) and an optimisation-based analysis step (blue). The main tools used for computation are OpenSim (dashed yellow box) and MATLAB (dashed purple box).

different metrics in numerous studies; however, most of them only focused on one single metric. Only a few studies have combined multiple metrics [10], [16], mostly employing a biomechanical model to obtain the solution space, rather than using directly a recorded variation of actual gait patterns as a solution space. Such an approach, however, makes personalisation a challenge. Furthermore, while applying fatigue modelling in the field of ergonomics has already been investigated [17], [19]–[21], applying fatigue as a metric in gait analysis and optimisation is still rather unexplored.

To address this literature gap, we created a modular framework for human gait performance analysis, which combines multiple metrics related to physical aspects: joint torque, manipulability, and fatigue. Joint torque was selected as a metric to allow modulation of instantaneous loads exerted on the joints, which is relevant in preventing the overloading of the musculoskeletal system. We selected manipulability because it gives an indication of how well the legs can produce or sustain motion and forces during different phases of the gait. Finally, to also account for the long-term walking endurance, fatigue was included. Although the major aspects of the gait are covered by these selected metrics, the proposed framework is general in the sense that, if needed, other metrics could be included.

II. Methods

A. The framework

An overview of the proposed framework is shown in Fig. 1. We employed motion capture experiments, including camera motion capture and GRFs, to collect variable gait patterns that served as a set for performance analysis based on the optimisation of metrics. We then used inverse kinematics and dynamics of the OpenSim biomechanical model [23] to transform the motion capture data into joint movements and torques needed for the calculation of the three key metrics considered in this study: joint torque, fatigue, and manipulability. Finally, we performed an analysis of variable gaits within the collected set via multi-metric optimisation. While the framework is general in the sense that 3D motion can be considered, in this study, we limited the analysis to the sagittal plane and we focused on six joints: hips, knees, and ankles (i.e., both legs).

B. Motion data acquisition

Since there is a wide variety of analysis goals that can be specified, a broad dataset with some degree of variation is preferred over a natural gait. Therefore, rather than studying the natural gait of several different subjects, we decided to study a broad set of gait variations created by one subject, since gait analysis is ideally subject-specific.

One of the reasons for choosing to work with experimentally collected data rather than simulated data is that experimentally collected data is already subject-specific and conforms with physiological feasibility and dynamic stability constraints. This approach is also common in the literature [24]. As human gait is an extremely complex movement with many possible optimal solutions, it is a challenge to create an analysis framework that delivers only feasible and subject-specific gait patterns in an efficient manner by using only simulations.

The gait recordings were performed using marker-based motion capture Qualisys (Sweden), which included 12 Oqus 700 infrared cameras for tracking the optical markers and two Oqus 210c cameras for recording video footage. The GRFs were measured using five force plates (KISTLER, Switzerland), which were laid down consecutively to form a sensorised walking platform. These data streams were acquired and synchronised by the software application Qualisys Track Manager. See Fig. 2 for an illustration of the setup.

The data acquisition was approved by the TU Delft Human Research Ethics Committee. The collected dataset contained gait patterns varying in stride length, step height, and walking speed. Each of these parameters could either have a low, medium or high value and a gait was recorded for each possible combination of these parameters, resulting in a total of 27 gait patterns. The naming convention used for the recorded gaits in the remainder of this paper is based

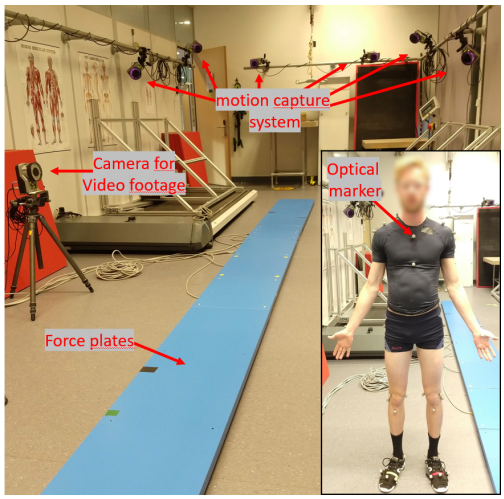

Fig. 2: Experiment setup including five force plates, 12 infrared cameras and two cameras for video footage. 44 optical markers were placed in several locations on the participant's body.

on these parameters, i.e., a gait with a low stride length, high step height, and a medium walking speed is named LowHighMid. It should be emphasised that only one of the recorded gaits was natural (MidLowMid). Additionally, some extra variations were included, i.e., walking with bent knees, leaning forward, and leaning backwards. This extra part of the dataset contained 18 gait patterns, thus adding up the total number of gaits in the dataset to 45.

C. Physical aspects

1) Joint torque: We used OpenSim software [23] to model the musculoskeletal variables and solve for the dynamics of the human body based on the motion capture and force plate recordings. The following equations of motion describe the simplified dynamics model:

$$\boldsymbol{\tau} = \boldsymbol{M}(\boldsymbol{q})\ddot{\boldsymbol{q}} + \boldsymbol{C}(\boldsymbol{q},\dot{\boldsymbol{q}})\dot{\boldsymbol{q}} + \boldsymbol{g}(\boldsymbol{q}) + \boldsymbol{J}^T(\boldsymbol{q})\boldsymbol{F_{ext}}, \quad (1)$$

where $\boldsymbol{\tau}$ are the joint torques, $\boldsymbol{q}$ and its derivatives are the generalised joint positions, velocities, and accelerations, $\boldsymbol{M}$ is the mass matrix, $\boldsymbol{C}$ is the Coriolis and centrifugal matrix, $\boldsymbol{g}$ is the vector of gravitational forces, $\boldsymbol{J}$ is the Jacobian matrix of the leg endpoint, and $\boldsymbol{F}_{ext}$ are the GRFs as recorded by the force plates.

The joint torque computed in (1) is used as one of the metrics in the analysis process (Section II-D; Fig. 1). The joint torque is also an input for the joint fatigue model (Section II-C.2). The Jacobian matrix $\boldsymbol{J}$ from (1) maps the GRFs to the body, and is also an important factor in the manipulability metric (Section II-C.3).

2) Joint fatigue: For the fatigue estimation, we used the model from [21], which is described as:

$$\frac{du_i(t)}{dt} = \begin{cases} (1-u_i(t))\frac{|\tau_i(\boldsymbol{q},t))|}{\lambda_i} & \text{if } |\tau_i(t)| \geq \tau_{th,i} \\ -u_i(t)\frac{R}{\lambda_i} & \text{if } |\tau_i(t)| < \tau_{th,i} \end{cases}, \quad (2)$$

where u_i is the fatigue index for the i-th joint, τ_i is the joint torque for the given time t, λ_i is the parameter that determines the joint-specific fatigue characteristics, R is the recovery rate, specifying how fast the joint recovers when it is resting. Whether the joint is in the resting state or not, is determined by the torque threshold $\tau_{th,i}$.

The recovery rate R was set to a conservative value of 0.5, as was also done in [17] and [21]. The parameter λ was determined after calibration experiments, similar to [17]. We used external force sensor measurements to estimate the joint torque, which was displayed in real-time on a screen. Two measurements were performed per joint, one for flexion and one for extension in the sagittal plane, thus 12 measurements in total. During each of these measurements, the subject was instructed to produce a reference torque τ_{ref} and try to maintain this torque level for as long as possible. The time T_{ref} was measured up to the point when the subject could not endure the torque level anymore. Note that this procedure is subject-dependant. Since the model follows an exponential charge function that mathematically never reaches the maximum value of 1, i.e., 100%, the maximum value of the joint fatigue parameter u was assumed to be reached after five time constants, thus when $u = 0.993$.

The fatigue capacity parameter λ was then derived for each joint (in both flexion and extension) by:

$$\lambda = -\frac{|\tau_{ref}| \cdot T_{ref}}{\ln(1-0.993)}. \quad (3)$$

The estimated parameters λ slightly differed between the same joints in the left and right legs. However, bilateral symmetry was assumed and the same λ value, corresponding to the weakest joint, was assigned to both sides. The weakest leg λ was selected to stay on the conservative side. This resulted in the set of λ parameters listed in Tab. I.

TABLE I: Joint-specific fatigue capacity λ and fatigue induction/recovery threshold τ_{th} parameters.

	Hip flexion	Hip extension	Knee flexion	Knee extension	Ankle dorsiflexion	Ankle plantarflexion
λ (Nms)	444	754	282	550	75.8	2.15e+3
τ_{th} (Nm)	0.177	-0.234	0.133	-0.184	0.046	-0.295

We defined the torque thresholds τ_{th} that determine whether the joints are increasing or decreasing their fatigue levels. Since the literature has not yet provided exact threshold values τ_{th} specifically for gait, we had to estimate those values based on experimental experience. During each of the fatigue calibration experiments, the subject was instructed to produce maximum torque with a specific joint. We assumed leg symmetry and for each joint type, the maximum torque of the weakest leg was assigned to that joint type in both legs. These maximum torques can be interpreted as an indication of the general strength of the joints with respect to each other. Finally, the torque thresholds were scaled to one another according to the ratio between these maximum torques.

The following assumption based on experimental experience was then made: after half an hour of regular walking, an average fatigue index of 20% is expected. It is fair to acknowledge that this was an ad-hoc value selected for the first step in this research direction (further discussed in Section IV). An initial guess was then made for the set

of torque thresholds based on their relationship calculated above, and the average fatigue index after 30 minutes was calculated. Then, depending on this value, the set of torque thresholds was adjusted. This process was iterated until an average fatigue level of 20% was reached, resulting in the set of thresholds listed in Tab. I.

3) Manipulability: We aimed at applying manipulability analysis on walking, in which several phases can be identified where the capability to produce motion is more relevant, and several phases where the propulsion or absorption of forces are more relevant. In robotics, manipulability can be visualised as an ellipse or ellipsoid for a 2D case or a 3D case, respectively. The length of the vector from the centre of the ellipse/ellipsoid to the surface indicates how well the limb can produce motion/forces in that specific direction of Cartesian space. In our 2D case, the principal axes of the manipulability ellipsoid were obtained by using singular value decomposition as:

$$\boldsymbol{U}\boldsymbol{\Sigma}\boldsymbol{V}^T = \boldsymbol{J}(\boldsymbol{q})\boldsymbol{J}(\boldsymbol{q})^T, \tag{4}$$

where $\boldsymbol{U}$ and $\boldsymbol{V}$ are matrices containing the left and right singular vectors respectively and $\boldsymbol{\Sigma}$ is a diagonal matrix containing the singular values. Since velocity and force manipulability are orthogonal to each other, the force manipulability is obtained by the inverse of (4).

The gait cycle can be divided into two main phases: stance and swing [25]. The stance phase is initiated by initial contact (IC), where the heel touches the ground (heel strike). The leg that touches the ground would be referred to as *leading leg* in this gait cycle. The stance phase can be further divided into loading response, mid-stance, terminal stance, and pre-swing. During the loading response, the impact of the foot on the ground is absorbed and the body's weight is transferred onto the leading leg. The mid-stance and terminal stance phases form the single-limb support phase, starting and ending when the non-leading leg leaves the ground (opposite toe-off (OTO)) and touches the ground again (opposite initial contact (OIC)), respectively. During those phases, the body weight is carried solely by the leading leg. The body is then propelled by the leading leg during pre-swing. Since each of these first four gait phases revolves around absorbing, carrying, or generating force, during these phases we put the focus on optimising force manipulability as seen in Tab. II. The swing phase can be divided into initial, mid-swing, and terminal swing. During the swing phase, the limb goes through three phases: lifting (initial swing), advancing (mid-swing), and preparing for the next stance phase (terminal swing). Since these phases focus on the advancement of the limb, during these phases we focused on optimising velocity manipulability. The gait phases were identified from a combination of motion capture and force plate data.

During the loading response, the contact with the ground of the leading leg is only through the heel, therefore, the heel was chosen as the endpoint for the force manipulability calculation during that phase. For mid-stance, when the body weight is slowly transferred from the heel towards the toe of the leading leg, the heel was also selected as the endpoint.

TABLE II: Overview of the selected leg endpoint manipulability type for each gait phase during the gait cycle.

Gait phase		Leg endpoint	Ellipse type
Stance phase	Loading response	Heel	Force
	Mid-stance	Heel	Force
	Terminal stance	Toe	Force
	Pre-swing	Toe	Force
Swing phase	Initial swing	Toe	Velocity
	Mid-swing	Toe	Velocity
	Terminal swing	Toe	Velocity

For all the other phases, the velocity manipulability and the force manipulability were calculated with the toe as the endpoint.

D. Multi-metric analysis based on optimisation of metrics

The framework aims to analyse and rank the gaits based on the optimisation of metrics. The input into the gait ranking process is the collected set of variable gait patterns $\mathcal{G}$ along with analysis goals in form of weights w on specific metrics, while the output is composed of ranked gaits according to the metrics. Ranking can be done recursively through optimisation as:

$$\arg\min_{\mathcal{G}_k} (T_{total} + U_{total} - S_{total} + O_{total}), \tag{5}$$

$$T_{total} = \sum_{i=1}^{n} (w_{t,i} \cdot T_i), \tag{6}$$

$$U_{total} = \sum_{i=1}^{n} (w_{u,i} \cdot U_i), \tag{7}$$

$$S_{total} = \sum_{j=1}^{m} (w_{s,j} \cdot S_j), \tag{8}$$

$$O_{total} = \sum_{j=1}^{m} (w_{o,j} \cdot O_j), \tag{9}$$

where $\mathcal{G}_k$ is the k-th gait pattern in the collected set $\mathcal{G}$, T_i and U_i are metrics representing the joint torque and joint fatigue for the i-th joint, respectively, S_j and O_j are metrics representing the manipulability ellipse shape and manipulability ellipse orientation for gait phase j, respectively, and $w_{t,i}$, $w_{u,i}$, $w_{s,j}$ and $w_{o,j}$ are weights corresponding to these metrics. The number of joints in the process is n (six: hips, knees, and ankles), and m is the number of gait phases (seven according to Tab. II). The ellipse shape S has a minus sign in the cost function since it has to be maximised, as opposed to the other metrics that have to be minimised. The metrics were normalised using the z-score normalisation method.

1) Selected metrics: The **joint torque metric** T for a joint i was defined as the mean absolute torque over one gait cycle:

$$T_i = \frac{1}{D} \sum_{t=0}^{D} |\tau_i(t)| dt, \tag{10}$$

where τ_i is the i-th joint torque at time t obtained from (1), dt is the sample time, and D is the duration of the gait cycle in number of samples.

The **joint fatigue metric** U for a joint i was defined as the fatigue level at the end of the gait cycle:

$$U_i = u_{i,D} \tag{11}$$

with $u_{i,D}$ representing the i-th joint fatigue index calculated from (2) after the duration of the gait cycle D.

The **manipulability metric** S **related to the ellipse shape** for gait phase j was defined as:

$$S_j = \frac{1}{D_j}\sum_{t=0}^{D_j} r(t)dt, \quad \text{with} \quad r(t) = \sqrt{\frac{\mu_1(t)}{\mu_2(t)}}, \tag{12}$$

where $\mu_1(t)$ and $\mu_2(t)$ are the major and minor singular values, respectively, at time instant t obtained from (4), and D_j is the duration of phase j in number of samples.

Finally, the **manipulability metric** O **related to the ellipse orientation** for gait phase j was defined as:

$$O_j = \frac{1}{D_j}\sum_{t=0}^{D_j} |\theta(t)|dt, \text{ with } \theta(t) = \tan^{-1}\left(\frac{v_{1,y}(t)}{v_{1,x}(t)}\right) - \theta_{ref} \tag{13}$$

where $v_{1,x}(t)$ and $v_{1,y}(t)$ are the x and y components of the singular vector v_1 at time instant t obtained from (4), which corresponds to the major axis of the velocity/force ellipse. The θ_{ref} is the desired reference orientation of the ellipse in a specific phase. Finally, $\theta(t)$ is the deviation angle between the major axis of the ellipse and the reference angle θ_{ref}.

For gait phases where the velocity ellipse was selected for optimisation, we chose θ_{ref} parallel to the ground and thus remains constant throughout the phase. In this way, velocity in the forward direction, i.e., the walking direction, is rewarded positively in the cost function. For gait phases where the force ellipse was selected for optimisation, θ_{ref} should ideally be aligned with the direction of the GRF, as done in [12]. In this case, the interaction forces can be absorbed optimally during the heel strike, and the foot can most efficiently propel the body off the ground during the toe-off. However, to simplify the computation and since visual inspection of the recorded motion data showed that the GRF could be assumed to point towards (or nearby) the pelvis, we defined θ_{ref} to be the angle between the selected endpoint (see Tab. II) and the pelvis. Since the leg is moving, the reference angle can change throughout the phase.

2) Optimisation algorithm: Since the main purpose of the proposed method is to analyse various gaits within the collected set, we applied a brute-force optimisation algorithm in order to go through all gaits in the set $\mathcal{G}$ and rank them. In practice, this means that the overall cost from (5) is computed for each recorded gait. Normally, the major drawback of this method is the lengthy computation time. However, as mentioned in Section II-B, the volume of the search space for the optimisation problem at hand is greatly reduced, as it is only filled with the variable gaits acquired by motion capture. Nevertheless, if the gait database eventually becomes much larger, another more efficient optimisation method could also be used. However, that would come at the expense of not going through all possible gaits within the library, thus limiting the scope of analysis.

III. Results

A. Effect of gait parameters on optimisation metrics

A subset of seven gaits was chosen from the recorded set $\mathcal{G}$ to display the effects of the gait parameters (stride length, step height, and walking speed) on the metrics (joint torque T, joint fatigue U, and manipulability ellipse shape S and orientation O). These gaits were: LowLowMid, MidLowMid, HighLowMid, MidMidMid, MidHighMid, MidLowLow, and MidLowHigh. We selected these gaits since this subset enables us to isolate the effect of altering one of the gait parameters while keeping the other two gait parameters constant, like this:

- Stride length: LowLowMid, MidLowMid, HighLowMid
- Step height: MidLowMid, MidMidMid, MidHighMid
- Walking speed: MidLowLow, MidLowMid, MidLowHigh

Note that the natural gait MidLowMid, defined by a medium stride length, low step height, and medium walking speed, is present in each row so that the observed results can always be compared to the natural gait.

Figure 3 shows the joint angles for the hip, knee, and ankle of the leading leg for one gait cycle, resulting from the inverse kinematics process in OpenSim. In each column, the natural gait is depicted (together with two other gaits), making it possible to compare each analysed gait to the natural gait. It can be observed, that a higher stride length results in a larger range of motion (ROM) for the hip, knee and ankle during the swing phase (toe-off (TO)-initial contact 2 (IC2)) and in a larger ROM for the ankle during the stance phase (IC-TO). Increasing the step height has the same effect on the hip and knee joints but an opposite effect on the ankle during the swing phase. During the stance phase, no difference in ROM is noticed for any joints. Altering the walking speed does not seem to have a clear effect on the joint angle trajectories.

B. Anlysis results

In Fig. 4, the force/velocity ellipses are visualised for each gait event during the gait cycle of the natural gait (MidLowMid). Only the analysis of this natural gait is shown to provide a general impression of the proposed analysis of the manipulability during normal walking. The ellipse shape S is quite comparable for most gait events, except for IC and OTO, where the ellipse is very stretched in the direction of GRF. Note that the lengths of the major axis of the manipulability ellipses in Fig. 4 were equalised for illustration purposes in order to put focus on the shape comparison (i.e., the ratio between the major and minor axis), rather than the actual size. In reality, major axes of IC and OTO are much larger compared to other events, due to the leg being in singular configurations.

We can see that the force ellipses, drawn for IC, OTO, heel rise (HR) and OIC, point very closely towards the pelvis, which is the reference point for the force ellipse orientation O during stance phase (as explained in Section II-D). For the velocity ellipses, drawn for TO, feet adjacent (FA), tibia

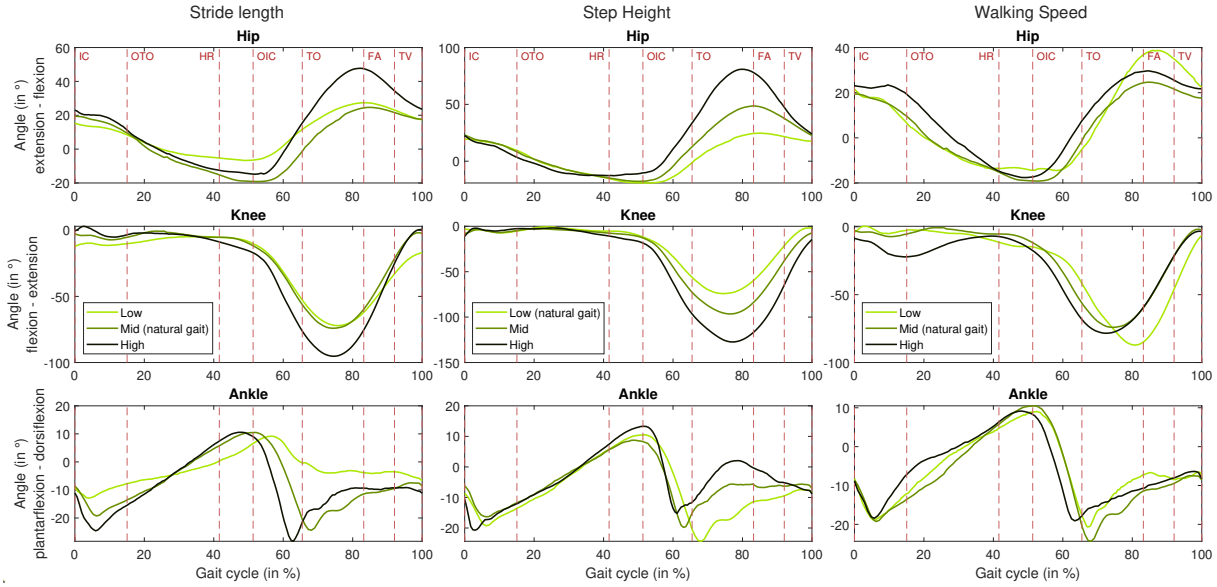

Fig. 3: The effect of the stride length (left column), step height (middle column), and walking speed (right column) on the joint angles during walking. To clarify: in the left column, LowLowMid, MidLowMid, and HighLowMid are depicted, in the middle column, MidLowMid, MidMidMid, and MidHighMid, and in the right column, MidLowLow, MidLowMid, and MidLowHigh. Relevant gait events are indicated by the red dashed lines. Note that these can slightly differ per gait, however only the gait events of the natural gait are shown to keep the figure organised.

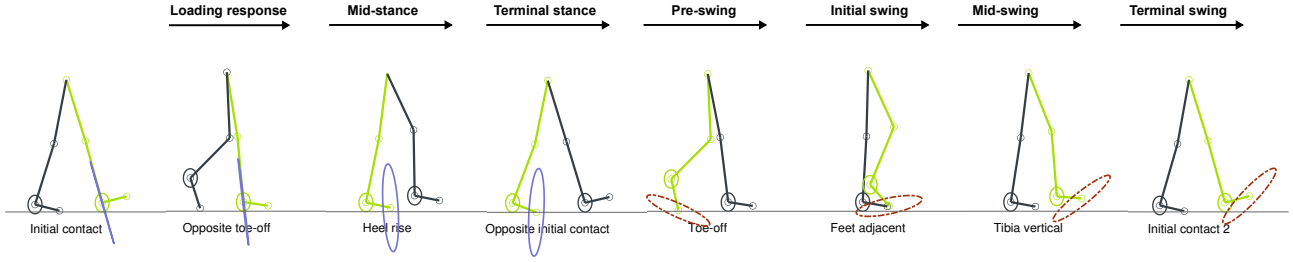

Fig. 4: The force ellipse (blue solid line) and velocity ellipse (red dashed line) for the relevant gait events of the natural gait MidLowMid. For easier illustration and comparison of the shape, the sizes of ellipses are scaled to have equally major axes. In the stance phase, i.e., IC until TO, the force ellipses are drawn, while in the swing phase, i.e., TO until IC2, the velocity ellipses are drawn. The dominant leg is indicated by green and the supporting leg by grey. Furthermore, the ellipses drawn for the gait events IC and OTO are centred on the heel, whereas the others are centred on the toe, as explained in Tab. II.

vertical (TV) and IC2, the reference direction for the ellipse orientation O is parallel to the ground (as explained in Section II-D). It can be observed that the velocity ellipse for FA points closely in this direction. For TO, TV and IC, the velocity ellipses have a larger deviation from this reference direction. Thus, in the case of the manipulability metric, natural gait is more optimal in some phases and less optimal in other phases.

Table III provides an overview of the total costs of each metric obtained by weighted sums from (6)-(9) and the overall cost obtained from (5) for each of the seven selected gaits. These costs were computed with all weights set to one, which provides a baseline/reference for gait analysis within the scope of this paper. These weights can be tuned to meet specific gait goals by future users of the framework.

TABLE III: Total costs per metric, together with the overall cost, given for the seven gaits treated in this section.

Gait	T_{total}	U_{total}	S_{total}	O_{total}	Overall cost
MidLowMid	-0.418	-0.459	0.18	-0.188	-0.885
MidLowLow	-0.215	-0.289	0.624	-0.34	-0.220
MidLowHigh	0.391	-0.280	0.0854	0.106	0.303
MidMidMid	-0.393	-0.508	-0.0587	-0.135	-1.09
MidHighMid	-0.268	-0.492	-0.28	-0.366	-1.41
LowLowMid	-1.16	-1.24	0.182	-0.499	-2.72
HighLowMid	-0.0759	-0.316	0.318	0.0263	-0.048

IV. Discussion

The results showed that different gait patterns end up with different total costs for the individual metrics, as well as for the overall cost (see Tab. III). Since the costs presented in this table are computed with all the optimisation weights set to one, these results function as a baseline for tuning the weights of the framework for the analysis of various goal-specific gaits. Furthermore, it can be used to analyse the gait patterns, in particular, to gain some insight into which aspect of the gait is responsible for a good or bad overall performance in terms of different metrics. For example, LowLowMid performs best in the baseline case, especially due to very low torque and fatigue costs, indicating that the joints are not loaded heavily and that this gait can be sustained for a long time. As LowLowMid is the gait with the least extreme leg configurations of the seven selected gaits (low stride length and low step height), this is to be

expected. When we look at MidHighMid, we observe a good performance in terms of manipulability. This indicates that this gait pattern offers leg configurations that are optimal for sustaining external loads during the stance phase and for advancing the limb during the swing phase.

The optimisation weights were intentionally set to one in this study in order for the results to function as a baseline analysis goal. However, the purpose of these weights is to provide a tool for the user to set various arbitrary analysis goals. Thus, further research into details of how to tune the weights for specific user requirements is needed.

In the computation of the torque thresholds and λ values for the fatigue model, bilateral symmetry of the legs was assumed, equalling both legs to the weakest one. Although bilateral symmetry might be a decent assumption in healthy individuals, there is typically a much larger difference in leg functionality for individuals with a physical leg injury or neurological injury [4]. In such cases, we want to minimise the risk of worsening the injury, and therefore, the conservative assumption of basing the fatigue characteristics of both legs on the capability of the weakest leg still seems like a good option. However, more research is needed in this direction.

Finally, to determine the torque threshold values, a fatigue index of 20% was assumed after half an hour of regular walking. Since no prior research has been performed suggesting a reasonable estimate of fatigue index after a specified walking time, an additional study is recommended to better calibrate the fatigue model.

V. Conclusion

The proposed framework was tested on a variety of recorded human gaits that were analysed with three metrics related to physical aspects of bipedal gait: joint torque, joint fatigue and leg manipulability. The method can help the users identify gaits that are most suitable for optimising these metrics. While the first step made by this study focused on humans, the approach can potentially be extended to humanoid robots, where we want to imitate human gaits [1], [2] or optimise specific characteristics of the robot's gait [3].

References

[1] W. Suleiman, E. Yoshida, F. Kanehiro, J.-P. Laumond, and A. Monin, "On human motion imitation by humanoid robot," in *2008 IEEE International conference on robotics and automation (ICRA)*, 2008, pp. 2697–2704.

[2] K. Miura, M. Morisawa, F. Kanehiro, S. Kajita, K. Kaneko, and K. Yokoi, "Human-like walking with toe supporting for humanoids," in *2011 IEEE/RSJ International Conference on Intelligent Robots and Systems (IROS)*, Sep. 2011, pp. 4428–4435.

[3] I. Lim, O. Kwon, and J. H. Park, "Gait optimization of biped robots based on human motion analysis," *Robotics and Autonomous Systems*, vol. 62, no. 2, pp. 229–240, Feb. 2014.

[4] L. Marchal-Crespo and D. J. Reinkensmeyer, "Review of control strategies for robotic movement training after neurologic injury," *Journal of NeuroEngineering and Rehabilitation*, vol. 6, no. 1, p. 20, Jun. 2009.

[5] A. Esquenazi, M. Talaty, A. Packel, and M. Saulino, "The ReWalk Powered Exoskeleton to Restore Ambulatory Function to Individuals with Thoracic-Level Motor-Complete Spinal Cord Injury," *American Journal of Physical Medicine & Rehabilitation*, vol. 91, no. 11, pp. 911–921, Nov. 2012.

[6] B. Chen, C.-H. Zhong, X. Zhao, H. Ma, X. Guan, X. Li, F.-Y. Liang, J. C. Y. Cheng, L. Qin, S.-W. Law, and W.-H. Liao, "A wearable exoskeleton suit for motion assistance to paralysed patients," *Journal of Orthopaedic Translation*, vol. 11, pp. 7–18, Oct. 2017.

[7] M. Tucker, E. Novoseller, C. Kann, Y. Sui, Y. Yue, J. W. Burdick, and A. D. Ames, "Preference-Based Learning for Exoskeleton Gait Optimization," in *2020 IEEE International Conference on Robotics and Automation (ICRA)*, May 2020, pp. 2351–2357.

[8] K. A. Ingraham, C. D. Remy, and E. J. Rouse, "The role of user preference in the customized control of robotic exoskeletons," *Science Robotics*, vol. 7, no. 64, p. eabj3487, Mar. 2022.

[9] J. Zhang, P. Fiers, K. A. Witte, R. W. Jackson, K. L. Poggensee, C. G. Atkeson, and S. H. Collins, "Human-in-the-loop optimization of exoskeleton assistance during walking," *Science*, vol. 356, no. 6344, pp. 1280–1284, Jun. 2017.

[10] C. L. Dembia, N. A. Bianco, A. Falisse, J. L. Hicks, and S. L. Delp, "Opensim moco: Musculoskeletal optimal control," *PLOS Computational Biology*, vol. 16, no. 12, p. e1008493, 2020.

[11] T. Yoshikawa, "Manipulability of Robotic Mechanisms," *The International Journal of Robotics Research*, vol. 4, no. 2, pp. 3–9, Jun. 1985.

[12] W. Kim, S. Lee, M. Kang, J. Han, and C. Han, "Energy-efficient gait pattern generation of the powered robotic exoskeleton using DME," in *2010 IEEE/RSJ International Conference on Intelligent Robots and Systems*, Oct. 2010, pp. 2475–2480.

[13] B. M. Fard and M. Mosadeghzad, "Manipulability Based Hierarchical Control of Perturbed Walking," *International Journal of Control, Automation and Systems*, vol. 17, no. 9, pp. 2343–2353, Sep. 2019.

[14] Z. Liu, L. Wang, C. L. P. Chen, X. Zeng, Y. Zhang, and Y. Wang, "Energy-Efficiency-Based Gait Control System Architecture and Algorithm for Biped Robots," *IEEE Transactions on Systems, Man, and Cybernetics, Part C (Applications and Reviews)*, vol. 42, no. 6, pp. 926–933, Nov. 2012.

[15] M. Peasgood, J. McPhee, and E. Kubica, "Stabilization and Energy Optimization of a Dynamic Walking Gait Simulation," in *International Design Engineering Technical Conferences and Computers and Information in Engineering Conference*. American Society of Mechanical Engineers Digital Collection, Jun. 2008, pp. 339–349.

[16] C. F. Ong, T. Geijtenbeek, J. L. Hicks, and S. L. Delp, "Predicting gait adaptations due to ankle plantarflexor muscle weakness and contracture using physics-based musculoskeletal simulations," *PLoS computational biology*, vol. 15, no. 10, p. e1006993, 2019.

[17] L. Peternel, N. Tsagarakis, D. Caldwell, and A. Ajoudani, "Robot adaptation to human physical fatigue in humanrobot co-manipulation," *Autonomous Robots*, vol. 42, no. 5, pp. 1011–1021, Jun. 2018.

[18] L. Ma, D. Chablat, F. Bennis, and W. Zhang, "A new simple dynamic muscle fatigue model and its validation," *International Journal of Industrial Ergonomics*, vol. 39, no. 1, pp. 211–220, Jan. 2009.

[19] P. Maurice, V. Padois, Y. Measson, and P. Bidaud, "Experimental assessment of the quality of ergonomic indicators for dynamic systems computed using a digital human model," *International Journal of Human Factors Modelling and Simulation*, vol. 5, no. 3, p. 190, 2016.

[20] M. Lorenzini, W. Kim, E. De Momi, and A. Ajoudani, "A new overloading fatigue model for ergonomic risk assessment with application to human-robot collaboration," in *2019 International Conference on Robotics and Automation (ICRA)*, 2019, pp. 1962–1968.

[21] L. Peternel, D. T. Schøn, and C. Fang, "Binary and Hybrid Work-Condition Maps for Interactive Exploration of Ergonomic Human Arm Postures," *Frontiers in Neurorobotics*, vol. 14, 2021.

[22] L. Peternel, N. Tsagarakis, and A. Ajoudani, "A method for robot motor fatigue management in physical interaction and human-robot collaboration tasks," in *2018 IEEE/RSJ International Conference on Intelligent Robots and Systems (IROS)*, 2018, pp. 2850–2856.

[23] A. Seth *et al.*, "OpenSim: Simulating musculoskeletal dynamics and neuromuscular control to study human and animal movement," *PLOS Computational Biology*, vol. 14, no. 7, p. e1006223, Jul. 2018.

[24] F. L. Haufe, S. Maggioni, and A. Melendez-Calderon, "Reference Trajectory Adaptation to Improve Human-Robot Interaction: A Database-Driven Approach," in *2018 40th Annual International Conference of the IEEE Engineering in Medicine and Biology Society (EMBC)*, Jul. 2018, pp. 1727–1730.

[25] D. Levine, J. Richards, and M. W. Whittle, *Whittle's Gait Analysis*. Elsevier Health Sciences, Jul. 2012.